International Journal of Engineering Innovation & Research
Volume 9, Issue 1, ISSN: 2277 – 5668

Anti-Hydroplaning Analysis of Tire Micro-Pattern Grooves

Yunfen Sun, Congzhen Liu *, Yongqiang Li, Yang Yuan, Mengyu Xie and Chengwei Xu
School of Transportation and Vehicle Engineering, Shandong University of Technology, 255049, Zhangdian district, Zibo city, Shandong province, China.
*Corresponding author email id: lcz200811@163.com

Date of publication (dd/mm/yyyy): 05/02/2020

Abstract **– The anti-hydroplaning performance of tires is mainly achieved by improving the drainage capacity of the tread pattern. The drag reduction and drainage increase of the pattern grooves are the keys to improve the hydroplaning performance of the tire. Improving drag reduction performance of tires without increasing pattern groove volume has become the focus of the research. Taking the tire single-pitch groove of 185/60R15 as the research object, and referring to the bionic design method, three types of microstructure grooves were arranged at the bottom of the tread pattern. At different water flow velocities, the computational fluid dynamics method was used to analyze the drag reduction and anti-hydroplaning performance of the grooves. The drag reduction effects of the three microstructure grooves are compared, and their drag reduction mechanisms are analyzed. The results show that three microstructures can reduce drag by increasing the thickness of the boundary layer, reducing wall shear stress and dynamic water pressure without increasing the groove volume. The first groove has a better drag reduction than others.**

Keywords **– Anti-Hydroplaning, Tread Pattern, Microstructure, Computational Fluid Dynamics, Drag Reduction Mechanism.**

I. INTRODUCTION

Once the speed is too high when the vehicle is driving on a wet road, the water in the ground contact area of the tire cannot be discharged from the pattern groove in time. The adhesion performance of the tire drops sharply, and the tire is prone to hydroplaning, which seriously affects the driving safety of the vehicle [1]. Therefore, it is very important to effectively improve the anti-hydroplaning performance of tires. In this regard, scholars have done a lot of research and achieved many valuable results [2-4]. One of the main factors that affect the anti-hydroplaning performance of the tire is the structural parameters of the tread pattern. B. Wies et al. [5] investigated the effect of the pattern structure and type on the hydroplaning performance through experiments, and the results showed that appropriately increasing the groove volume especially the central groove could improve the tire's hydroplaning performance.

In recent years, bionic technology has been preliminarily used to solve problems in the fluid engineering field [6-7]. The research [8] found that there were grooves on shark scales in the same direction as water flow and applied this drag reduction structure to the spacecraft. Test results show that the bionic grooves reduced the spacecraft drag force by 5.6%. Bechert D.W. et al. [9] conducted wind tunnel tests by simulating the three-dimensional (3D) rib structure on the surface of the shark, and found that the 3D rib surface could produce a considerable drag reduction effect, and the turbulent shear stress was reduced by 7.3% compared with the smooth flat plate. Huiming Li et al. [10] found that rib grooves on the surface of transverse dolphins have drag reduction effect on both laminar flow and turbulence. The bionic drag reduction technologies provide inspirations to improve the anti-hydroplaning ability of tires.

Research shows that microstructure grooves are important for fluid drag reduction. Based on the groove of shark skin, this study designed three kinds of bionic microstructure. Three kinds of microstructural grooves were

arranged at the bottom of the single-pitch pattern groove according to the characteristics of groove reducing viscosity and decreasing drag to fluid. Through computational fluid dynamics numerical simulation, the effects of three microstructure grooves on the flow resistance and the tread groove drainage capacity were studied. Analysis of the drag reduction mechanism of the grooves proves the effectiveness of the anti-hydroplaning ability without changing the grooves volume.

II. Establishment the Pattern Groove Model with Microstructure

A. *Tire Model*

Type 185/65 R15 radial tire was selected with the standard pressure of 210 kPa and the standard load of 3920 N. The finite element model is shown in Fig. 1. The size of the longitudinal groove with single pitch in the middle part of contact patch is 8 mm depth, 30 mm long and 7 mm wide. Because of the main drainage function is achieved by the longitudinal pattern grooves, single pitch longitudinal pattern groove in the middle of contact patch was researched.

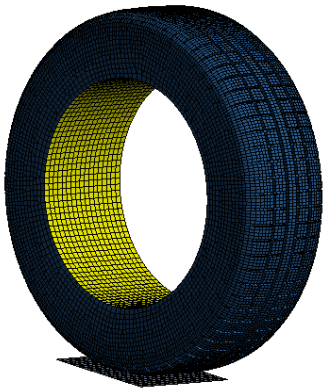

Fig. 1. Finite element model of tire.

B. *Patterned Groove Model with Microstructural Groove*

Using the concept of bionic microstructure drag reduction, three kinds of microstructure grooves were designed. The three kinds of microstructural grooves were arranged at the bottom of the pattern grooves using ANSYS and shown in Fig. 2. They have same radius *r* but with different transition sections. For groove I, semicircles are tangential. The transition sections of grooves II and III are straight line and arc, respectively.

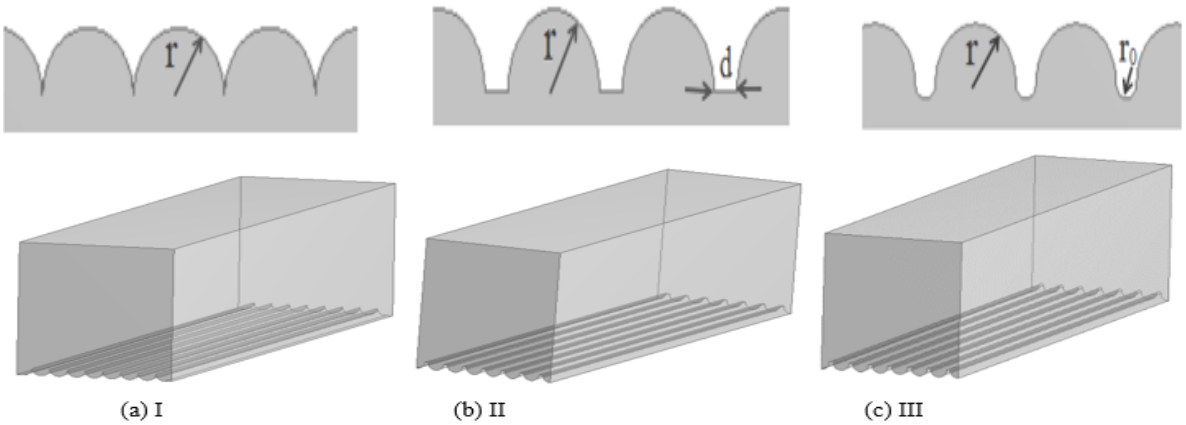

Fig. 2. Model of single pitch patterned groove with different microstructure.

The drag reduction of microstructure is mainly achieved by influencing the burst structures in the fluid boundary layer and increasing the thickness of the viscous bottom layer. Therefore, the theory of fluid boundary layer thickness should serve as basis of estimating the size of the groove of microstructure. According to the fluid boundary layer theory [11], the calculation formula of boundary layer thickness is:

$$\delta = 0.381 L R\mathrm{e}^{-1/5} \tag{1}$$

Where L is the characteristic length and Re is the Reynolds number. The Reynolds number Re is related to the velocity, density, viscosity coefficient and characteristic length of the fluid. After calculation, the maximum boundary layer thickness of the fluid in the pattern groove is about 0.918 mm. In order to ensure that the non-smooth microstructure can influence the internal structure of the boundary layer, the size of the microstructure should not be too close to the thickness of the boundary layer [12]. Therefore, the grooves radius r of the model is set to 0.4 mm, the transition line d of the groove II is 0.2 mm, and the transition arc radius r_0 of the groove III is 0.1 mm.

C. *Mesh of the Computational Domain*

The calculation domain of pattern groove is meshed by the mesh editing component that comes with Fluent software, and the method of combining structured grid with unstructured grid was adopted. In order to capture the characteristics of water flow movement in the near-wall area, mesh refinement should be carried out in the near-wall area. The mesh thickness of the first layer is related to the value of dimensionless y^+. The viscous bottom of the boundary layer is about $0 \le y^+ \le 5$ (y^+ is the dimensionless distance of the wall), so the dimensionless number of the first grid near the wall must be controlled within $y^+ \le 5$. The grid thickness of first layer near the wall (y) is obtained by the following formula:

$$\mathrm{y} = \frac{\mu y^+}{C_\mu^{1/4} \kappa_p^{1/2}} \tag{2}$$

Where y^+ is the dimensionless distance from the first grid to the wall surface; μ is the dynamic viscosity of the fluid; C_μ is the empirical constant that equal to 0.09 usually; k_p is the turbulent kinetic energy of the first node [13]. Finally, after repeated attempts, the mesh thickness of the first layer is 0.01 mm, the growth rate is 1.2, and the maximum mesh size of the computing domain is 0.25 mm, as shown in Fig. 3. In addition, in the simulation analysis of the pattern groove model, it is assumed that the inflow water is an isothermal and incompressible viscous fluid. Standard k - ε model is selected as turbulence model, and the SIMPLE format is selected as the numerical solution method for flow field.'

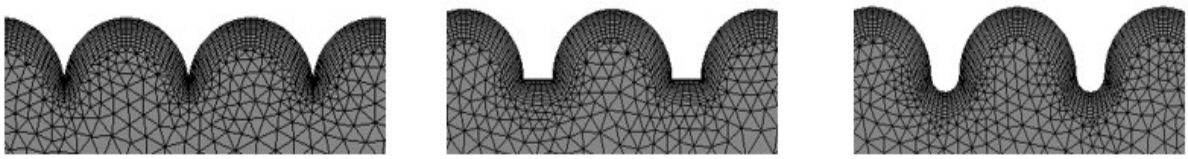

Fig. 3. Schematic diagram of local meshes of three microstructure grooves.

D. *Boundary Condition*

Set the boundary conditions of the three models with microstructure grooves in the ANSYS workbench Fluent module.

Inlet conditions: the inlet of the flow-groove fluid domain was set as the velocity inlet to study the drag reduction effect of three microstructures at different flow rates. Four initial inlet velocities were considered to be 70 km/h, 80 km/h, 90 km/h and 100 km/h, respectively.

Outlet conditions: set the outlet of the fluid field as the pressure outlet.

Wall boundary conditions: the wall surfaces of the pattern groove were set to be Static without slip.

III. Analysis of Flow Characteristics in Tire Groove

The hydrodynamic pressure can be obtained from Bernoulli equation that is the difference between the total pressure and the velocity pressure at a certain point in the pipeline when water is flowing. Utilizing the Bernoulli equation of steady flow:

$$P+\rho gh+\frac{1}{2}\rho v^2=C \tag{3}$$

When the fluid flows horizontally, Bernoulli equation can be expressed as:

$$P+\frac{1}{2}\rho v^2=C \tag{4}$$

Where P is the hydrodynamic pressure; ρ is the density of water; V is the velocity of water; C is a constant. According to the above equation, the consumption of velocity is converted into dynamic pressure. The frictional resistance will be greater when the dynamic pressure be the higher and the velocity be lower. The hydrodynamic pressure of each micropattern groove at different speeds was simulated by Fluent software, as shown in Table 1.

Table 1. Hydrodynamic pressure of each micro-pattern groove at different speeds.

V / (km/h)	Category	P / kPa
70	Original groove	117.882
	Groove I	43.382
	Groove II	43.393
	Groove III	45.056
80	Original groove	160.133
	Groove I	60.719
	Groove II	62.518
	Groove III	64.037
90	Original groove	241.364
	Groove I	82.629
	Groove II	83.725
	Groove III	87.038
100	Original groove	264.789
	Groove I	101.137
	Groove II	113.823
	Groove III	115.121

It can be seen from table 1 that with the increase of water flow speed, the hydrodynamic pressure of each pattern increases. Under the same inflow speed, the hydrodynamic pressure of the three microstructured grooves are much smaller than that of the original grooves, and the hydrodynamic pressure of groove I is the smallest. The results show that non-smooth microstructure can reduce the flow resistance and hydrodynamic pressure.

In order to explore the drag reduction effect of microstructure non-smooth surface on tire groove, the drag reduction rate R was set as the test index. R is the drag reduction rate of non-smooth surface compared to smooth surface. The calculation formula was as follows:

$$R = \frac{(\tau_s - \tau_g)}{\tau_s} \times 100\% \tag{5}$$

Where, τ_s and τ_g are the shear stresses of the original pattern groove and the pattern groove with microstructure, respectively. If $R > 0$, it means that the microstructure groove has drag reduction effect, and the greater the absolute value be, the more obvious drag reduction effect becomes. If $R < 0$, it indicates that the microstructure groove has the resistance increasing characteristic, and the larger the value be, the more obvious the resistance increasing effect becomes. If $R = 0$, it indicates that the microstructure groove has neither drag reduction effect nor drag increasing characteristic. The drag reduction effect of each model at different speeds is shown in Table 2.

Table 2. Drag reduction rates of microstructures at different flow rates.

Speed (km/h)	Scheme	Wall shear stress (Pa)	Drag-reduction efficiency (%)
70	Original groove	766.42	0
	Groove I	520.47	32.09
	Groove II	650.30	15.15
	Groove III	723.54	5.59
80	Original groove	992.47	0
	Groove I	668.27	32.67
	Groove II	833.26	16.04
	Groove III	940.89	5.20
90	Original groove	1374.33	0
	Groove I	854.44	37.83
	Groove II	1021.63	25.66
	Groove III	1165.45	15.20
100	Original groove	1519.69	0
	Groove I	997.93	34.33
	Groove II	1289.08	15.17
	Groove III	1404.62	7.57

It can be seen from Table 2 that all three kinds of microstructure grooves have the effect of drag reduction. With the increase of speed, drag reduction increases first and then decreases. Comparing the three structures, it is found that the drag reduction efficiency of groove I is the best, groove II is the second, and groove III is the worst.

IV. Analysis of Drag-Reduction Mechanism of Microstructure

When the speed is 90 km/h, the drag reduction capacity of each groove is better than other speeds. Taking the velocity as an example, through analyzing of the wall shear stress contour, velocity contour and velocity vector of each groove, the drag reduction mechanism of three kinds of microstructure surfaces is explored.

A. *Wall Shear Stress Contour Analysis*

The analysis and comparison of the pattern groove wall shear stress contour are shown in Fig. 4.

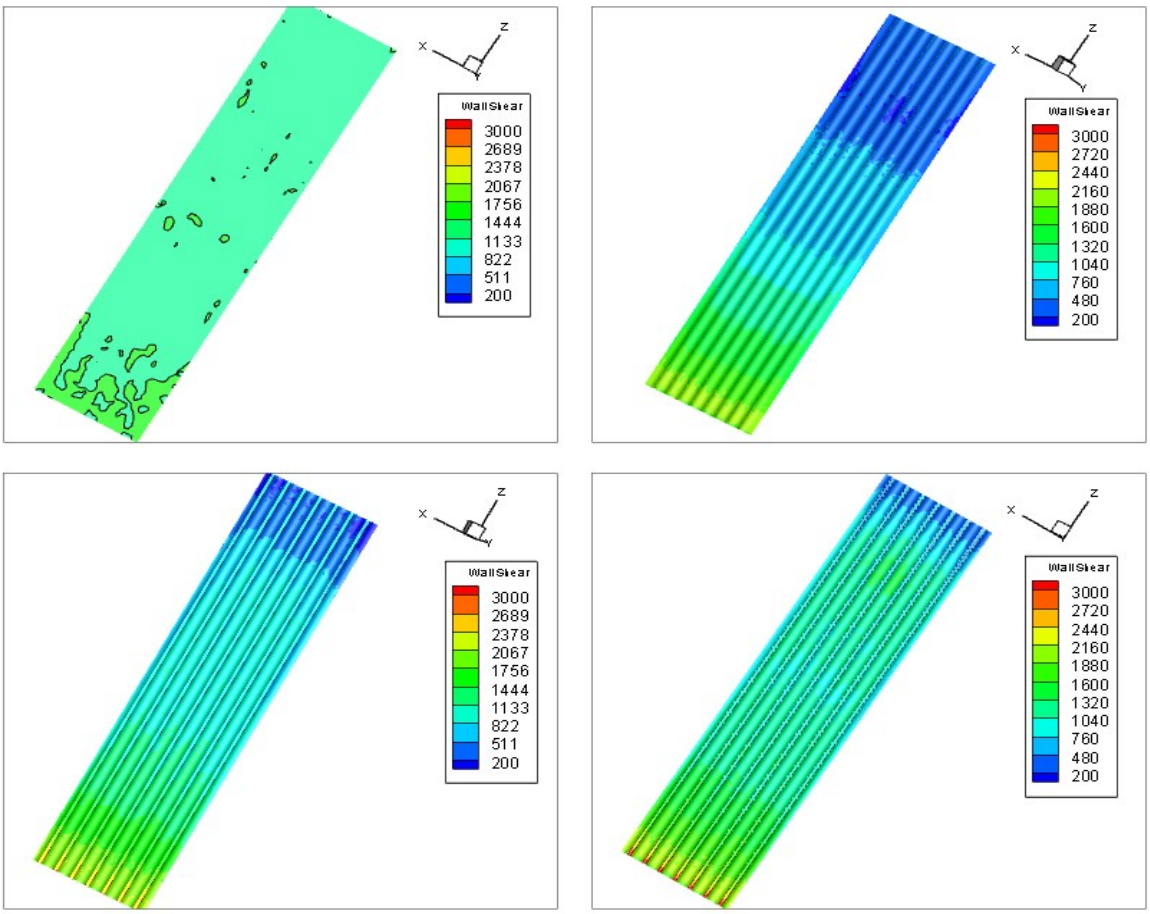

Fig. 4. Comparison of wall shear stress.

The reduction of resistance is mainly achieved by a large reduction of viscous resistance. The shear stress on the wall can reflect the viscous resistance of the fluid. It could be found from the comparison diagram of the shear stress that the micro-structure grooves are more stressed than the original grooves. The reason why fluid flowing in the inlet has not stabilized. But as the microstructure begins to function, the flow field gradually turns to a steady state, and the shear stress value of the fluid gradually decreases. Finally, it is much smaller than the original groove to achieve drag reduction. Compared with the wall shear stress value at the entrance and the area occupied by low shear stress, it can be seen that the wall stress of groove I is smaller than the other two. Therefore, three kinds of grooves can reduce the wall shear stress, and the effect of groove I is the best.

B. *Velocity Contour Analysis*

In order to avoid the influence of entrance and exit effects, the flow velocity contour of cross section 15 mm away from the entrance was selected for analysis.

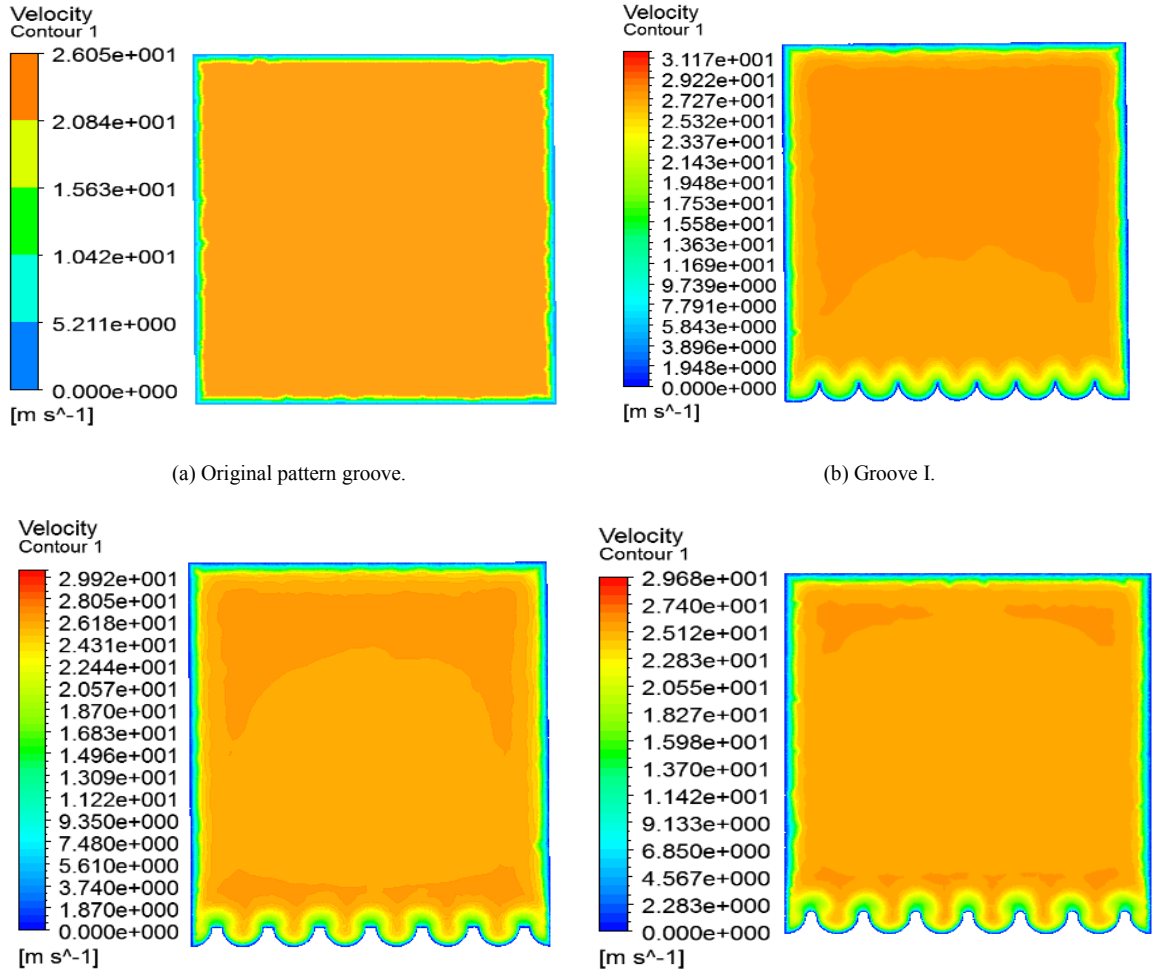

(a) Original pattern groove.

(b) Groove I.

(c) Groove II.

(d) Groove III.

Fig. 5. Comparison of velocity distribution in the feature plane Z = 15 mm.

Fig. 5 shows that the velocity field of smooth groove is quite different from that of other micro structure grooves. The boundary layer of the original groove is very thin, and the velocity reaches the mainstream velocity in the boundary layer. The velocity gradient is large and changes violently. Due to the existence of the micro-grooves, the thickness of the boundary layer of the pattern groove is raised to a certain extent, so that the groove is located in the low-speed flow field at the bottom of the boundary layer. The three microstructure grooves are surrounded by low-speed fluid, the velocity gradient is reduced significantly, and the friction resistance is reduced effectively. The drag reduction is achieved by increasing the thickness of the wall boundary layer and reducing the velocity gradient of the viscous bottom layer. It can be seen from the observation that the boundary layer thickness and the main flow velocity of the three grooves are different. The boundary layer of groove I is thick and uniform, and the main flow velocity is large, so the drag reduction effect is the best.

C. *Velocity Vector Analysis*

The following is the velocity vector of the longitudinal section of the pattern groove, as shown in Fig. 6.

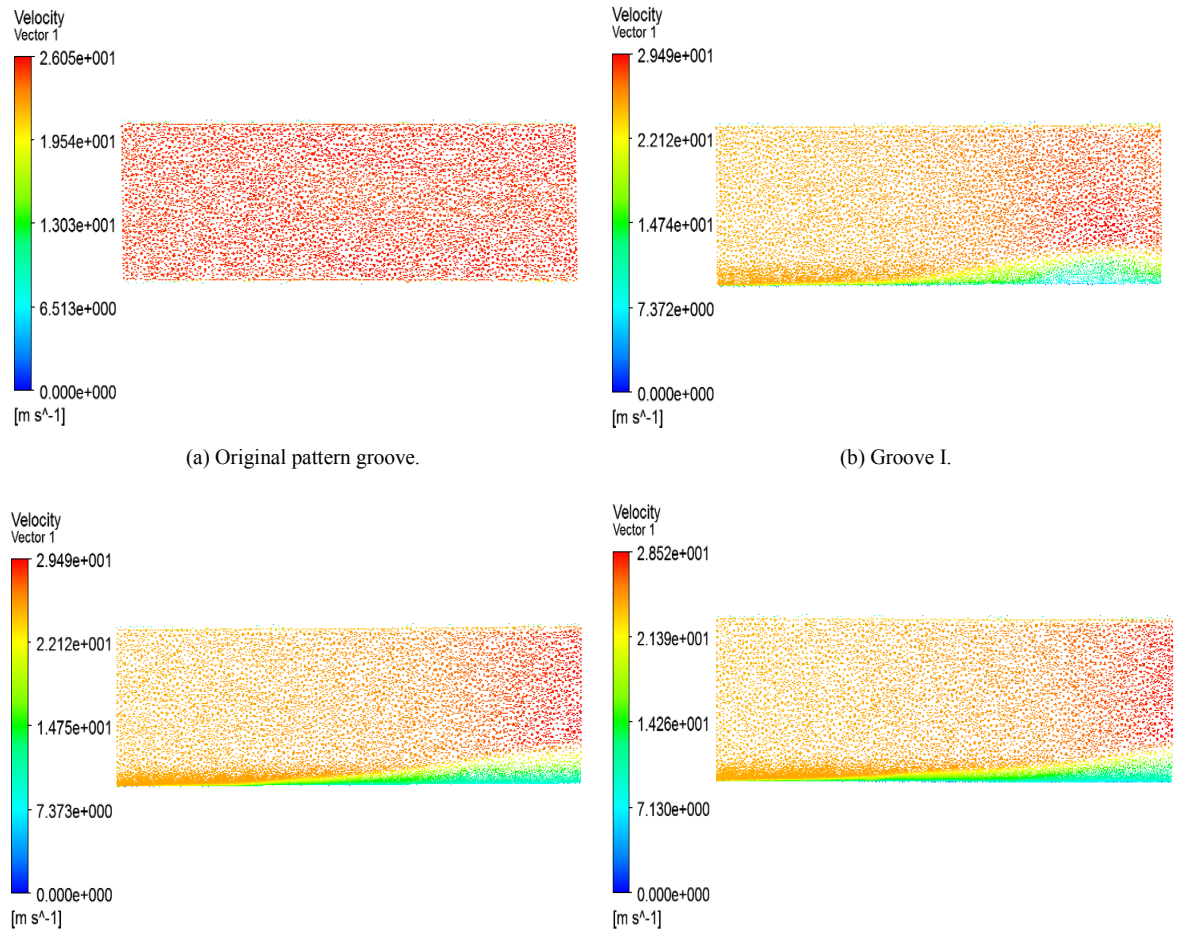

(a) Original pattern groove. (b) Groove I.

(c) Groove II. (d) Groove III.

Fig. 6. Velocity vector of longitudinal section.

It can be seen from the comparison that there are lots of low-speed fluid at the bottom of the groove with pattern groove, and the flow is relatively gentle. The fluid with high flow velocity is located above the groove, so it is difficult to sweep the bottom of the groove, so the shear stress value is low. As the fluid gets farther from the pattern grooves entrance, the thickness of the low-speed fluid becomes higher. The higher the thickness of vulgar fluid is, the faster the flow rate of fluid above it will increase the drainage speed of the grooves. Secondly, the existence of grooves can limit the translation of eddy, reduce the interaction of eddy, reduce the probability of the large eddy's occurrence, and achieve the effect of drag reduction. By comparing the thickness of low-speed fluid and the value of high-speed fluid, it can be seen that the drag reduction effect of groove I is better.

V. Conclusion

In this paper, the design of the tread groove of the tire is carried out by the bionic shark skin, and the flow characteristics and drag reduction mechanism of each groove are analyzed by FLUENT software. The conclusions are as follows:

Firstly, the numerical analysis of the hydrodynamic pressure and drag reduction rate of different grooves, it is shown that the tire grooves with microstructure can effectively reduce the flow resistance and increase the drainage capacity of the groove. With the increase of the speed, the drag reduction effect increases first and then decreases. When the speed is 90 km / h, the drag reduction ability of each groove is better than other speeds.

Secondly, the resistance reduction analysis of the microstructure groove, it is found that the three kinds of grooves have different drag reduction effects. Groove I has the best drag reduction effect and groove III has the worst drag reduction effect. The results show that the smaller the distance between microgrooves is, the better the drag reduction effect becomes.

Finally, the microstructure groove can avoid excessive wall energy consumption and reduce friction resistance by increasing wall boundary layer thickness. It improves the mainstream velocity of the fluid in the grooves and improves the anti-hydroplaning performance of the tire.

REFERENCES

[1] Yiyang Yang, Nan Xu, Konghui Guo, et al. Application of hydroplaning mechanism in high-speed steel trip tire test rig. Journal of Jilin University : Engineering and Technology Edition, (46), 2016, pp. 7.
[2] S.S. Kumar, A. Kumar, T.F. Fwa. Analyzing effect of tire groove patterns on hydroplaning speed. Journal of the Eastern Asia Society for Transportation Studies, 8, 2009, pp. 2018-2031.
[3] T. Okano, M. Koishi. A new computational procedure to predict transient hydroplaning performance of a tire. Tire Science and Technology, 29(1), 2001, pp. 2-22.
[4] Tianjian Ji, Xiaoming Huang, Qingquan Liu. Influence of part hydroplaning on road adhesion coefficient. Journal of Traffic and Transportation Engineering, 3(4), 2003, pp. 10-12.
[5] B. Wies, B. Roeger, R. Mundl. Influence of Pattern Void on Hydroplaning and Related Target Conflicts. Tire Science and Technology, 37(3), 2009, pp. 187-206.
[6] Peng Cui, Zhi Chen, Xiaochao Zhang. Statics analysis of apple-picking robot humanoid manipulator. Transaction of the Chinese Society for Agricultural Machinery, 42(2), 2011, pp. 149-153.
[7] Jie Li, Jide Zhuang, Dong Wei, et al. Comparative traction performance tests between bionic camel foot tire and common tire. Journal of Jilin University: Engineering and Technology Edition, 36(04), 2006, pp. 510-513.
[8] Walsh, J. Michael. Riblets as a viscous drag reduction technique. Aiaa Journal, 21(4), 1983, pp. 485-486.
[9] D.W. Bechert, D.W. Bruse, W. Hage. Experiments with three-dimensional riblets as an idealized model of shark skin. Experiments in Fluids, 28(5), 2000, pp. 403-412.
[10] Huiming Li. Direct numerical simulation of drag reduction of underwater aircraft and drag reduction mechanism analysis. Harbin Institute of Technology, 2006.
[11] Jing Luo, Yundong Li. Approximate solution of mixing boundary layer's ply on flat plate. Journal of Science of Teachers' College and University, (02), 2009, pp. 54-56.
[12] J. Sun, C.J. Nappo, L. Mahrt, et al. Review of wave-turbulence interactions in the stable atmospheric boundary layer. Reviews of Geophysics, 53(3), 2015, pp. 956-993.
[13] Tianran Li. Numerical study of bionic surface for drag reduction. Dalian University of Technology, 2012.

AUTHOR'S PROFILE

First Author
Yunfen Sun, She was born in Shandong Province, PRC in December1994. She studies in Shandong University of Technology (Shandong, PRC) from Sept 2018 to now, major in Transportation and Vehicle Engineering. Shandong University of Technology, 255049, Zhangdian district, Zibo city, Shandong province, China.

Second Author
Congzhen Liu, Male, Associate professor, Doctor of Engineering, School of Transportation and Vehicle Engineering, Shandong University of Technology, 255049, Zhangdian district, Zibo city, Shandong province, China.
email id: lcz200811@163.com

Third Author
Yongqiang Li, Male, School of Transportation and Vehicle Engineering, Master in reading, Shandong University of Technology, 255049, Zhangdian district, Zibo city, Shandong province, China. email id: lyq961210@163.com

Fourth Author
Yang Yuan, Male, Master in reading, School of Transportation and Vehicle Engineering, Shandong University of Technology, 255049, Zhangdian district, Zibo city, Shandong province, China.

Fifth Author
Mengyu Xie, Male, Master inreading, School of Transportation and Vehicle Engineering, Shandong University of Technology, 255049, Zhangdian district, Zibo city, Shandong province, China.

Sixth Author
Chengwei Xu, Male, Master in reading, School of Transportation and Vehicle Engineering, Shandong University of Technology, 255049, Zhangdian district, Zibo city, Shandong province, China.